Cerebral Cortex, July 2018;28: 2253–2266

doi: 10.1093/cercor/bhx126
Advance Access Publication Date: 17 May 2017
Original Article

ORIGINAL ARTICLE

Atypical Endocannabinoid Signaling Initiates a New Form of Memory-Related Plasticity at a Cortical Input to Hippocampus

Weisheng Wang[1], Yousheng Jia[1], Danielle T. Pham[1], Linda C. Palmer[1], Kwang-Mook Jung[1], Conor D. Cox[1], Gavin Rumbaugh[2], Daniele Piomelli[1,3,4,5], Christine M. Gall[1,6] and Gary Lynch[1,7]

[1]Department of Anatomy and Neurobiology, University of California, Irvine, CA 92697, USA, [2]Department of Neuroscience, The Scripps Research Institute, Jupiter, FL 33458, USA, [3]Department of Pharmacology, University of California, Irvine, CA 92697, USA, [4]Department of Biological Chemistry, University of California, Irvine, CA 92697, USA, [5]Drug Discovery and Development, Instituto Italiano di Tecnologia, 16163 Genoa, Italy, [6]Department of Neurobiology and Behavior, University of California, Irvine, CA 92697, USA and [7]Department of Psychiatry and Human Behavior, University of California, Irvine, CA 92697, USA

Address correspondence to Christine M. Gall and Gary Lynch, Department of Anatomy and Neurobiology, University of California at Irvine, 837 Health Science Road, Irvine, CA 92697, USA. Email: cmgall@uci.edu (C.M.G.); Email: ga.s.lynch@gmail.com (G.L.)

Abstract

Endocannabinoids (ECBs) depress transmitter release at sites throughout the brain. Here, we describe another form of ECB signaling that triggers a novel form of long-term potentiation (LTP) localized to the lateral perforant path (LPP) which conveys semantic information from cortex to hippocampus. Two cannabinoid CB_1 receptor (CB_1R) signaling cascades were identified in hippocampus. The first is pregnenolone sensitive, targets vesicular protein Munc18-1 and depresses transmitter release; this cascade is engaged by CB_1Rs in Schaffer–Commissural afferents to CA1 but not in the LPP, and it does not contribute to LTP. The second cascade is pregnenolone insensitive and LPP specific; it entails co-operative $CB_1R/\beta1$-integrin signaling to effect synaptic potentiation via stable enhancement of transmitter release. The latter cascade is engaged during LPP-dependent learning. These results link atypical ECB signaling to the encoding of a fundamental component of episodic memory and suggest a novel route whereby endogenous and exogenous cannabinoids affect cognition.

Key words: cannabinoid receptor 1, lateral perforant path, long-term potentiation, Munc18-1, pregnenolone

Introduction

The granule cells of the hippocampal dentate gyrus (DG) are densely innervated by the superficial layers of the lateral and medial entorhinal cortices (Amaral and Lavenex 2007), which convey information about the nature of cues and their location in space (Eichenbaum and Fortin 2005). The granule cells then relay information to the CA3 pyramidal cells that generate a massive associational (CA3–CA3) system (Witter 2007); recording studies from rodents suggest that this region incorporates data relating to when the cues occurred (Salz et al. 2016). CA3 also gives rise to the very large Schaffer–Commissural (S–C) projection to pyramidal neurons in field CA1, where further integration likely occurs. CA1 directly and through intermediaries innervates the deep layers of entorhinal cortex (Amaral and Lavenex 2007). It is widely held that through this circuitry the hippocampus converts a sequence of inputs from cortex into representations that

include semantic, spatial, and temporal components (Aggleton and Brown 1999; Eichenbaum 2000). Multiple studies suggest that transmission of this code back to cortex is essential for the construction and retrieval of episodic memory, a fundamental ingredient of orderly thought (Eichenbaum et al. 2012).

Consistent with this role, each of the above hippocampal connections undergoes stable potentiation of synaptic transmission, long-term potentiation (LTP), following brief periods of afferent stimulation including activity patterns exhibited during learning. Much has been learned about the synaptic events that induce, express, and rapidly consolidate the potentiated state, particularly for the CA3–CA1, S–C connection: enduring changes occur postsynaptically and involve reorganization of the spine cytoskeleton, enlargement of the postsynaptic density, and an increase in membrane neurotransmitter receptors (Lynch et al. 2007, 2013; Granger and Nicoll 2014). Appreciation of how hippocampus executes its memory encoding operations will depend on the extent to which other connections in the circuit use this or other forms of plasticity. Recent work suggests that pronounced pathway-specific differences are in fact present. Specifically, the lateral perforant path (LPP) afferents from lateral entorhinal cortex to the DG exhibit a form of potentiation that depends on postsynaptic induction but is expressed presynaptically as an increase in evoked transmitter release (Wang et al. 2016). The retrograde messenger required by this arrangement proved to be the endocannabinoid (ECB) 2-arachidonoylglycerol (2-AG) which is synthesized in dendritic spines and diffuses to CB_1 receptors (CB_1Rs) on axon terminals. The 2-AG system is present at many types of synapses where its direct retrograde signaling has been shown to transiently depress release (Diana and Marty 2004; Castillo et al. 2012); nevertheless, it serves the very different purpose of promoting potentiation of transmission in the LPP.

Recent studies demonstrated that presynaptic signaling through ERK1/2 to the vesicular protein Munc18-1 is critical for CB_1R-mediated depression of release (Schmitz et al. 2016). Here, we show that CB_1R agonists readily activate this signaling cascade at S–C synapses but not in the LPP. Instead, at LPP terminals the CB_1R/2-AG system is biased toward a second cascade involving β1 integrins and presynaptic actin regulatory signaling. The finding that a specialized form of synaptic potentiation is used to encode semantic information processed by hippocampus calls for substantial revisions to current hypotheses about how the structure contributes to the formation of memory. It also provides a new perspective for understanding the abnormal encoding of episodes produced by cannabinoid drugs.

Materials and Methods

All studies used male rats and mice that were group housed (≤5 per cage) on a 12 h on/12 h off light cycle with food and water ad libitum. Excepting animals used for behavioral studies, the lights were turned on at 6:30 AM; for behavioral groups lights were turned on at 8 PM. Experiments were initiated from 8 to 10 AM for electrophysiology and for treatments leading to biochemical measures, and from 9 to 10 AM for behavioral studies. All animals were naïve to treatment prior to the procedures described.

Hippocampal Slices and Extracellular Field Recordings

Animals used for extracellular field recordings were 5- to 8-week-old male rats (Sprague–Dawley; Harlan Laboratories) and mice. The mice included (1) Munc18-1 heterozygote knockouts (KOs) (Munc18-$1^{+/-}$; a.k.a. STXBP1 from Riken labs) and background strain (C57BL/6N) matched wild types for comparison, and (2) conditional β1-integrin KOs created by crossing mice with floxed β1-integrin exon 3 with mice expressing Cre-recombinase under control of the CaMKIIα promoter (Mortillo et al. 2012; Wang et al. 2016a); in the progeny the expression of Cre by excitatory hippocampal and cortical neurons (Tsien et al. 1996) leads to excision of β1 exon 3 and disruption of β1 protein expression beginning at 3 weeks of age. The present studies used β1 KOs at 8 weeks of age. The preparation of hippocampal slices and their maintenance in an interface recording chamber has been described in detail elsewhere (Trieu et al. 2015; Wang et al. 2016). Animals were killed by decapitation under deep isofluorane anesthesia and the brain was quickly submerged into oxygenated, ice-cold, high-magnesium artificial cerebral spinal fluid (ACSF) containing (in mM): 124 NaCl, 3 KCl, 1.25 KH_2PO_4, 5 $MgSO_4$, 26 $NaHCO_3$, and 10 dextrose. For rats, slices from the middle third of the hippocampal septo-temporal axis were sectioned at a thickness of 330–400 μm using a McIlwain tissue chopper; for mice 375 μm thick sections were prepared on the horizontal plane using a Leica Vibrating Slicer (Model: VT1000S). In both cases, slices were collected into oxygenated, high-magnesium ACSF and then transferred onto an interface recording chamber (31 ± 1 °C; 95% O_2/5% CO_2) and continuously perfused with preheated oxygenated ACSF containing (in mM): 124 NaCl, 3 KCl, 1.25 KH_2PO_4, 1.5 $MgSO_4$, 26 $NaHCO_3$, 2.5 $CaCl_2$, and 10 dextrose at a rate of 60–70 ml/h. Experiments were initiated about 1.5 h after slices were placed on the recording chamber.

Field excitatory postsynaptic potentials (fEPSPs) were recorded by positioning a glass recording electrode (filled with 2M NaCl; 2–3 MΩ) and bipolar stimulating electrode (twisted nichrome wire 65 μm) in 2 hippocampal pathways (Trieu et al. 2015). For studies of the LPP innervation of the DG, recording and stimulating electrodes were both positioned in the outer molecular layer (internal blade), adjacent to the hippocampal fissure. All evoked responses were initially tested with paired-pulse stimuli (40 and 200 ms interpulse interval) to confirm specificity of potentials and thus electrode placement: LPP responses show paired-pulse facilitation whereas the adjacent medial perforant path shows paired-pulse depression (Christie and Abraham 1994). For studies of S–C innervation of field CA1 stratum radiatum, recording and stimulating electrodes were positioned in CA1b and CA1c, respectively, at comparable distance from the pyramidal cell layer. Test pulses were delivered at 0.05 Hz and baseline stimulation intensity was adjusted to 50–60% of the maximum spike-free fEPSP. Stable baseline recordings were collected for at least 20 min prior to pharmacological manipulation or induction of LTP. For the LPP, LPT was induced using 1 of 2 paradigms: (1) two 100 Hz trains, lasting 1 s and separated by 1 min with stimulus duration and intensity increased to 100% and 50% above baseline levels, respectively, and (2) one 100 Hz train, lasting 1 s, no current changes (termed "threshold level" stimulation). Stimulus strength was returned to baseline levels after induction. LTP in field CA1 was induced using one 100 Hz trains, lasting 1 s. The level of potentiation was assessed using 0.05 Hz pulses (i.e., baseline stimulation parameters) delivered for ≥1 h after inducing stimulation.

In all instances, initial slopes and amplitudes were measured from digitized fEPSPs (NACGather 2.0, Theta Burst Corp.) and normalized to mean responses over the last 20 min of the baseline period. Assessments of the level of potentiation were made for the period from 50 to 60 min after delivery of the inducing 100 Hz stimulation. For analysis of pharmacological treatment effects on synaptic responses, statistical tests

considered slice mean responses over the last 5 min of the recording period unless otherwise specified.

Whole-Cell Recordings

Hippocampal slices were prepared on the horizontal plane at a thickness of 370 μm from 3- to 4-week-old male rats with a Leica vibrating tissue slicer (Model: VT1000S). Slices were placed in a submerged recording chamber and continuously perfused at 2–3 mL/min with oxygenated (95% O_2/5% CO_2) at 32 °C. Whole-cell recordings (Axopatch 200A amplifier: Molecular Devices) were made with 4–7 MΩ recording pipettes filled with a solution containing (in mM): 130 $CsMeSO_4$, 10 CsCl, 8 NaCl, 10 HEPES, 0.2 EGTA, 5 QX-314, Mg-ATP, 0.3 Na-GTP. Osmolarity was adjusted to 290–295 mOsm and pH 7.4. Bipolar stimulating electrodes were placed in the outer molecular layer to stimulate the LPP. Excitatory postsynaptic currents (EPSCs) were recorded by clamping the granule cell at −55 mV and confirmed with AP5 and CNQX application. Inhibitory postsynaptic currents (IPSCs) were recorded at holding potential of 0 mV and confirmed with bicuculline application.

Drug Application

For hippocampal slice experiments, compounds were introduced to the bath (6 mL/h) via an independent perfusion line using a syringe pump (KD Scientific). Field recording studies used the CB_1R inverse agonist AM251 (5 μM), CB_1R agonist WIN 55, 212–2 mesylate (5 μM), H1152 (0.1 μM), focal adhesion kinase (FAK) Inhibitor 14 (Y15, 40 μM), GM 6001(25 μM), physostigmine hemisulfate (10 μM), and pregnenolone sulfate sodium salt (10 μM), purchased from Tocris Bioscience. The latter 2 were dissolved in water; others were dissolved in dimethyl sulfoxide (DMSO) and diluted in ACSF to achieve the final concentration and ≤0.01% DMSO in the ACSF bath. Integrin-targeted reagents were applied locally by pressure ejection (Kramar et al. 2003); these included echistatin (E1518, Sigma-Aldrich, 10 μM) and neutralizing antisera to β1 and αV integrin (MAB1987Z and CBL1346Z, respectively; 0.2 mg/mL; EMD Millipore). For some experiments, GABAA receptor antagonist picrotoxin (PTX) (Sigma-Aldrich) was introduced to the slice bath via the main ACSF perfusion line. For intraperitoneal injections, rats were given AM251 (1 mg/kg, 40 min before test) dissolved in DMSO, cremophore, ethanol, 0.9% saline (1:1:1:17) or vehicle.

Lipid Quantification

Levels of 2-AG, oleoylethanolamide (OEA), arachidonic acid, and stearic acid were determined using liquid chromatography/mass spectrometry (LC/MS) methods (Jung et al. 2007). For analysis of effects of physostigmine treatment, the hippocampal slices were quickly snap-frozen and then homogenized in methanol containing appropriate internal standards. Protein concentration was determined using the bicinchoninic acid protein assay (Pierce). Lipids were extracted with chloroform, and further fractionated by open-bed silica gel column chromatography. The eluates were dried under N_2 and reconstituted in chloroform/methanol for LC/MS analyses as described (Jung et al. 2012). To quantify levels of 2-AG and OEA, we used an Agilent 1200 LC system coupled to a 6410 triple quadrupole MS system (Agilent Technologies). Lipids were separated using a XDB Eclipse C18 column (50 × 4.6 mm i.d., 1.8 μm, Zorbax, Agilent), eluted with a gradient of methanol in water (from 90% to 100% in 5 min, to 100% in 7 min, and to 90% in 8 min) at a flow rate of 1 mL/min. Column temperature was held at 40 °C. MS detection was in electrospray ionization (ESI) and positive ionization mode, with capillary voltage at 3.5 kV and fragmentor voltage at 135 V. N2 was used as drying gas at a flow rate of 12 L/min and temperature of 350 °C. Nebulizer pressure was set at 50 psi. Quantifications were conducted by an isotope dilution method, monitoring [M+H]+ in the selected ion monitoring (SIM) mode. The multiple reaction transitions monitored were as follows: 2-AG, m/z 379→287; $^2H_8$-2-AG, *m/z* 387→295; OEA, *m/z* 326→62; $^2H_4$-OEA, *m/z* 330→66 (*m/z*, mass-to-charge ratio). Detection and analysis were performed using Mass Hunter Workstation software (Agilent). Levels for free fatty acids were determined by LC/MS methods (Jung et al. 2007) using an Agilent 1100-LC system (Agilent Technologies) coupled to a 1946A-MS detector equipped with ESI interface (Agilent Technologies). For fatty acids, mobile phase A consisted of methanol containing 0.25% acetic acid and 5 mM ammonium acetate; mobile phase B consisted of water containing 0.25% acetic acid and 5 mM ammonium acetate. We used a reversed-phase Zorbax XDB Eclipse C18 column (50 × 4.6 mm i.d., 1.8 m, Agilent Technologies) eluted with a linear gradient from 90% to 100% of A in B for 2.5 min at a flow rate of 1.5 mL/min with column temperature at 40 °C. ESI was in the negative mode, capillary voltage was set at 4 kV, and fragmentor voltage was 100 V. N_2 was used as drying gas at a flow rate of 13 L/min and a temperature of 350 °C. Nebulizer pressure was set at 60 psi. Fatty acids are measured by monitoring the mass-to-charge ratio (*m/z*) of deprotonated molecular ions $[M\text{-}H]^-$ in SIM mode: for oleic acid, *m/z* = 281 and for heptadecanoic acid, *m/z* = 269. We used commercially available fatty acids as reference standards. Detection and analysis were performed using Agilent Chemistation and Bruker Daltonics software. Calibration curves were generated using commercial fatty acids. Limit of quantification was 0.5 pmol.

Fluorescence Deconvolution Tomography/ Quantification of Immunolabeling

Measures were collected from hippocampal slices given either LTP-inducing or low-frequency stimulation (LFS), and from brains of animals given odor discrimination training. For the slice studies, the tissue was immersion fixed in 4% paraformaldehyde and sectioned (20 μm) on a freezing microtome, and then the top 6 sections (from the surface of electrode placement) were slide mounted and processed for immunofluorescence (Seese et al. 2012). For behavioral studies, rats were euthanized immediately after the last trial and brains were then quickly frozen in 2-methylbutane (−55 °C), cryostat-sectioned (20 μm), and 3 sets of tissue sections were collected with 300 μm spacing between sections in each set. Separate spans of sections were collected from the septal, mid-septo-temporal, and temporal regions of hippocampus, with the section angle adjusted for each to remain approximately perpendicular to the long axis of hippocampus. The microscope slide mounted tissue was fixed in 4% paraformaldehyde and processed for immunostaining as described (Seese et al. 2014). Immunofluorescence procedures used cocktails of primary antisera (Table 1) including rabbit antisera to pMunc18-1 Ser241 (Schmitz et al. 2016), phosphorylated proline-rich tyrosine kinase 2 (pPyk2) Tyr402 (Zhao et al. 2000), phosphorylated RhoA associated coiled coil containing kinase 2 (pROCK2) Ser1366 (Chuang et al. 2012), or pFAK Y397 (Bock and Herz 2003), used in combination with mouse antisera to synaptophysin (SYN) (Wen et al. 2014) or postsynaptic density protein-95 (PSD-95) (Takahashi et al. 2011); or guinea pig anti-vGluT2 used in combination with rabbit anti-CB_1 (Matyas et al. 2006) that was generously

Table 1. Primary antisera used

Antigen	Concentration	Source	Catalog #	RRID
Integrin β1	0.2 mg/mL	EMD Millipore	MAB1987Z	AB_94494
Integrin αV	0.2 mg/mL	EMD Millipore	CBL1346Z	AB_11212409
pMunc18-1 Ser241	1:500	PhosphoSolutions	p1305-241	AB_2492155
pPyk2 Tyr402	1:500	ThermoFisher Scientific	44-618G	AB_2533697
pROCK2 Ser1366	1:500	GeneTex	GTX122651	AB_2560946
pFAK Y397	1:500	ThermoFisher Scientific	44-624G	AB_2533701
CB_1R	1:5000	Provided by K. Mackie		
vGluT2	1:8000	Synaptic Systems	#135404	AB_887884
SYN	1:1000	EMD Millipore	MAB5258	AB_2313839
PSD-95	1:1000	ThermoFisher Scientific	MA1-045	AB_325399

provided by Dr Ken Mackie of Indiana University. Secondary antisera from ThermoFisher Scientific included Alexa Fluor 594 anti-rabbit IgG (A21207), Alexa Fluor 488 anti-mouse IgG (A21202) and Alexa Fluor 488 anti-guinea pig IgG (A-11073) all used at 1:1000 dilutions.

An epifluorescence microscope (Leica DM6000) with a 63× PlanApo objective and ORCA-ER camera (Hamamatsu) was used to capture image z-stacks, through a depth of 2 μm in 0.2 μm z-steps, from the DG outer molecular layer and CA1 stratum radiatum. For slice experiments, 1 z-stack was captured from each of 6 sections per slice. For behavioral/brain studies, 3 z-stacks were captured per section from 3 to 4 spaced sections within a given septo-temporal span of hippocampus (described above). Immunolabeling for the synaptic vesicle protein SYN and for the excitatory synapses postsynaptic scaffold protein PSD-95 served as markers for the presynaptic and postsynaptic compartment, respectively. The incidence and density of immunolabeling for the phosphoprotein co-localized with these compartment markers were then evaluated using wide-field epifluorescence microscopy and fluorescence deconvolution tomography (FDT) as described elsewhere (Seese et al. 2012, 2013). Briefly, images within each z-stack were processed for iterative deconvolution (99% confidence, Volocity 4.0, PerkinElmer) and then used to construct a 3-dimensional (3D) montage of the sample field. Automated systems (Rex et al. 2009; Seese et al. 2012) were then used to normalize background density, identify immunolabeled elements within the size and eccentricity constraints of synapses, and quantify (count and measure fluorescence intensity) those double-labeled. Elements were considered double-labeled if there was any overlap in the field labeled with the 2 fluorophores as assessed in 3D.

Odor Discrimination Behavior

Male Long–Evans rats (6–10 week old) were handled for 6 sessions, 2 sessions per day, and prior to odor discrimination training. Procedures for animal handling, training, and testing were adapted from Martens et al. (2013) as described in detail elsewhere (Wang et al. 2016). Sessions of ten 30 s trials on a given odor pair were repeated up to twice daily until rats reached a success rate of 80% correct (i.e., selection of the odor scented cup associated with a food reward) at which point they were considered to have acquired the odor discrimination task. On the following day, trained rats were either given 10 training trials on a novel odor pair (learning group) or transported to but not placed in the test apparatus (control group), and killed immediately thereafter for tissue harvest (ten trials are sufficient for rats that have acquired the task to learn a novel odor pair; Wang et al. 2016).

Statistical Analyses

All results are presented as means ± SEM. Statistical significance ($P < 0.05$) was evaluated using Student's *t*-test, 1-way or 2-way analysis of variance (ANOVA) with a Bonferroni post hoc test. In all cases analyses used Prism software (GraphPad) that provides evaluation of the suitability of the test for the specific data set.

Results

CB_1R / Munc18-1 Signaling is Markedly Different in 2 Hippocampal Pathways

The CB_1R is found on axon terminals throughout the brain (Katona et al. 2006; Uchigashima et al. 2011) including the field of LPP termination in the outer molecular layer of the DG (Wang et al. 2016). We confirmed CB_1R localization to glutamatergic (i.e., VGluT2 immunopositive [+]) terminals in the rat LPP field and then compared the effects of cannabinoid receptor agonist WIN 55,212–2 (WIN) on synaptic physiology in the S–C and LPP projections. In accord with prior work (Paton et al. 1998; Schmitz et al. 2016), WIN (5 μM) caused a rapid and pronounced depression of S–C fEPSPs in CA1 ($P < 0.0001$; Fig. 1*a*) that was accompanied by an increase in paired-pulse facilitation ($P = 0.0067$; Fig. 1*b*) and the expected severe impairment of LTP ($P < 0.0001$; Fig. 1*c*). Very different results were obtained in the LPP: WIN had no effect on baseline fEPSPs or on paired-pulse facilitation (Fig. 1*d*,*e*). Voltage-clamp recordings also detected no effect on EPSCs in the LPP (see Supplementary Fig. S1). In contrast to these results for glutamatergic responses in the LPP, WIN produced the canonical depression of IPSCs elicited by single pulse LPP stimulation ($P = 0.0004$; Fig. 1*f*). We next asked if, despite the lack of effect on baseline responses, WIN influences the machinery that produces the ECB-dependent potentiation of the LPP (*lpp*LTP) using stimulation that is near threshold for induction. WIN more than doubled the magnitude of *lpp*LTP under these conditions ($P = 0.0054$; Fig. 1*g*). These results suggest that activation of CB_1Rs in the LPP preferentially engages signaling mechanisms leading to potentiated transmission as opposed to the more commonly observed depression of release.

CB_1R signaling through ERK1/2 effects phosphorylation and degradation of the vesicular protein Munc18-1 leading to reductions in transmitter release (Schmitz et al. 2016). In accord with this, using dual immunofluorescence and FDT (Fig. 1*h*), we found that treatment with WIN increased levels of phosphorylated (p) Munc18-1 S241 co-localized with the presynaptic marker SYN in the S–C terminal field: WIN caused both a rightward shift in the pMunc18-1 immunolabeling intensity-frequency distribution ($P < 0.0001$; Fig. 1*i*) and increased

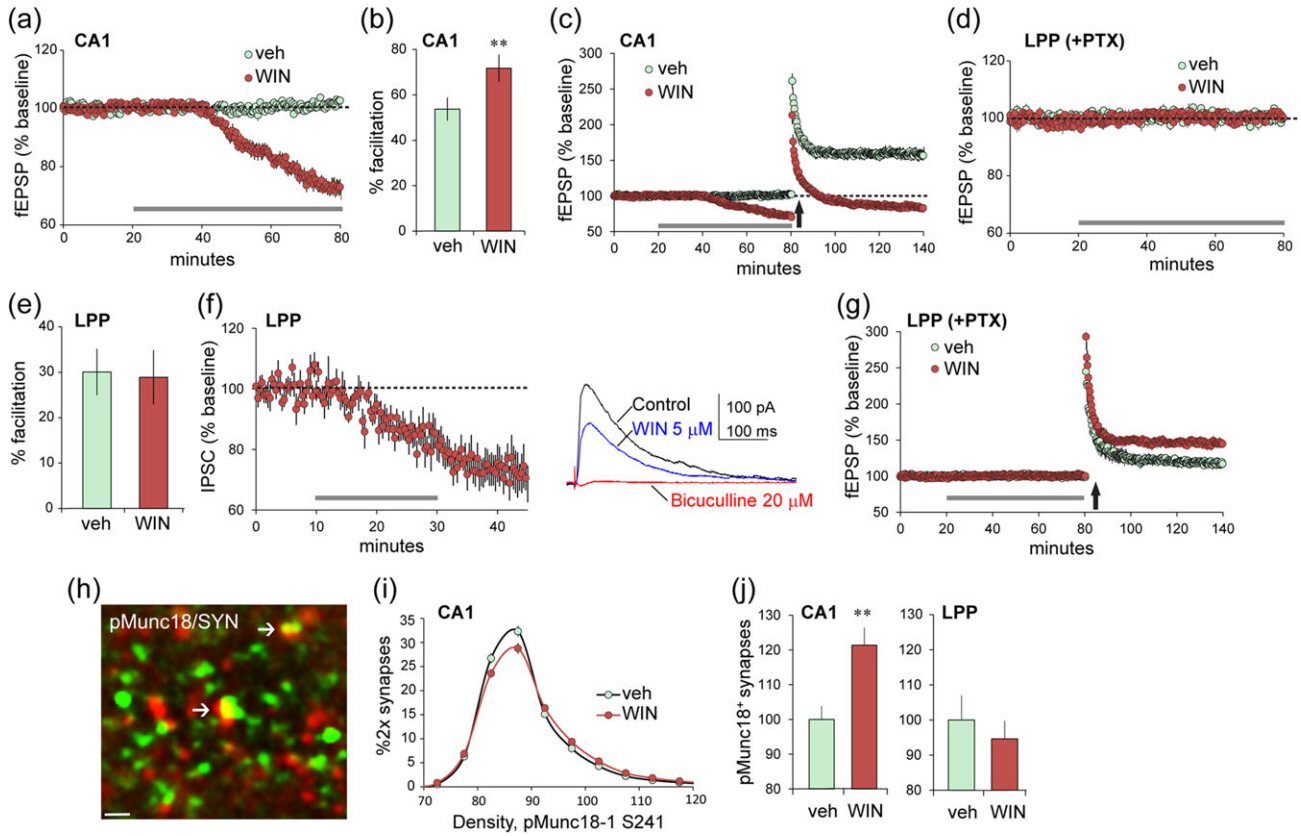

Figure 1. Projection-specific differences in synaptic CB_1R signaling and function. (*a–c*) Field recordings of S–C responses in acute hippocampal slices. (*a*) Infusion of cannabinoid receptor agonist WIN (5μM) (horizontal gray bar), compared with vehicle depressed baseline S–C synaptic responses ($P < 0.0001$, $t_{(11)} = 12.60$ in *a–g*, and *i*), (*b*) increased the magnitude of paired-pulse facilitation (**$P = 0.0067$, $t_{(12)} = 3.27$; 40 ms interpulse interval), and (*c*) blocked potentiation of transmission induced by HFS ($P < 0.0001$, $t_{(11)} = 6.64$; HFS applied at upward arrow). (*d–g*) Recordings of LPP responses were collected from the DG outer molecular layer. (*d*) Infusion of WIN in the presence of 100 μM PTX had no effect on LPP baseline responses ($P = 0.23$, $t_{(11)} = 1.27$) or (*e*) paired-pulse facilitation ($P = 0.88$, $t_{(12)} = 0.15$; 40 ms interpulse interval). (*f*) Voltage-clamp recordings (HP = 0 mV) show that WIN attenuates IPSCs recorded from DG granule cells with LPP stimulation ($P = 0.0004$, $t_{(10)} = 5.15$; mean ± SEM for 6 cells). Traces are representative responses collected before (control) and 20 min after WIN infusion onset. Later elimination of the response by bicuculline confirmed it was GABA receptor-mediated. (*g*) WIN infusion (at bar) enhanced the magnitude of *lpp*LTP induced with near threshold stimulation with 100 μM PTX present ($P = 0.0054$, $t_{(11)} = 3.45$). (*h,i*) Representative deconvolved image shows localization of pMunc18-1 S241 in a subset of SYN+ terminals in CA1. Plot shows the intensity-frequency distribution for pMunc18-1 immunofluorescence in SYN+ terminals (*h*): WIN caused a modest right shift denoting increased presynaptic immunoreactivity (i; 2-way ANOVA, $P < 0.0001$, $F_{19,342} = 5.54$). (*j*) Numbers of terminals with intense pMunc18-1 immunoreactivity (>100 units fluorescence intensity) for the CA1 S–C field (left) and the DG LPP field (right): WIN increased the numbers of densely pMunc18-1+ terminals in CA1 (**$P = 0.0037$, $t_{(18)} = 3.33$) but not in the LPP ($P = 0.87$, $t_{(18)} = 0.62$). LTP was evaluated 55–60 min after induction in *a–g*. Group sizes: $n = 6$ for veh and $n = 7$ for WIN in *a–g* and $n = 10$ in *h* and i; 2-tail *t*-test unless specified.

numbers of terminals with dense pMunc18-1 immunoreactivity ($P = 0.0037$; Fig. 1*j* left). In the same slices, WIN had no effect on presynaptic pMunc18-1 immunolabeling in the LPP terminal field (Fig. 1*j* right).

The above results indicate that WIN-initiated CB_1R signaling at LPP terminals is biased "away from" the ERK1/2-to-Munc18-1 cascade through which ECBs suppress neurotransmitter release and toward a route that promotes plasticity. They also raise the question of whether signaling to Munc18-1 and release suppression in CA1 is engaged by normally occurring patterns of physiological activity. Blocking the CB_1R with the inverse agonist AM251 had no effect on S–C fEPSPs elicited by single pulses (0.05 Hz). Thus, we tested for an effect using short trains of low-frequency gamma (40 Hz) stimulation. This pattern occurs routinely in hippocampal and entorhinal fields in behaving animals and is thought to be associated with processing of complex information (Colgin 2015). Within-slice comparisons were made between responses collected before and after 40 min perfusion of vehicle or 5 μM AM251. In CA1, S–C responses to low gamma stimulation showed the rapid, within-train frequency facilitation described in prior work (Trieu et al. 2015) (Fig. 2*a*). AM251 did not affect baseline responses but clearly enhanced S–C response facilitation during the gamma train (mean facilitation over the last five pulses; $P = 0.021$; Fig. 2*b*). Effects of AM251 were greatest in later portions of the train, as anticipated for contributions of "on-demand" ECB production. Very different results were obtained for the LPP. Within-train facilitation was less pronounced in the LPP than in the S–C system, and this effect was not altered by AM251 (Fig. 2*c,d*). These findings are consistent with the hypothesis that CB_1R signaling leading to a depression of transmitter release is more readily engaged in the S–C projections than in the LPP.

Pregnenolone-Sensitive Munc18-1 Phosphorylation does not Contribute to *lpp*LTP

The above results were unexpected because prior studies showed that physostigmine causes a suppression of excitatory transmission in the LPP and other hippocampal pathways that is blocked by AM251 (i.e., it is CB_1R-dependent) (Colgin et al. 2003).

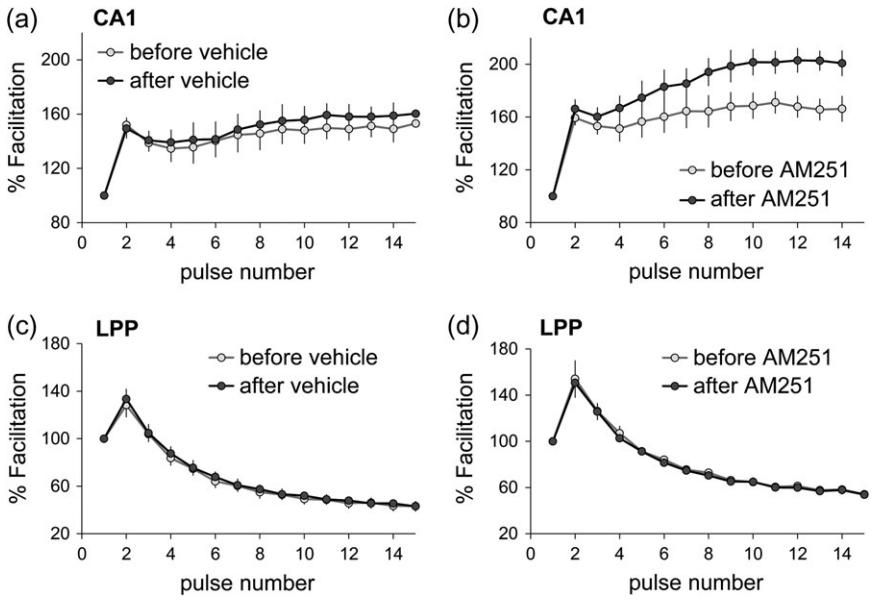

Figure 2. Projection-specific role of CB_1R in synaptic responses produced by low-frequency gamma stimulation. Short (400 ms) trains of 40 Hz stimulation were applied to field CA1 S–C projections or the LPP before and after inclusion of vehicle (*a* and *c*) or CB_1R inverse agonist AM251 (5μM; *b*, and *d*) in the tissue bath. Plots show the percent fEPSP facilitation across the train with values normalized to the first fEPSP. (*a* and *b*) In CA1, AM251 had no effect on the initial within-train facilitation but significantly potentiated fEPSPs later in the train ($P = 0.021$, $t_{(8)} = 2.87$). (*c* and *d*) Neither vehicle (*c*) or AM251 (*d*) influenced within-train LPP responses (pulses 2–6: $P = 0.79$, $t_{(8)} = 0.270$; pulses 10–15: $P = 0.83$, $t_{(8)} = 0.217$). $n = 15$ slices/field; all 2-tailed *t*-test.

Therefore, we tested if physostigmine increases hippocampal 2-AG levels, as anticipated, and then used the FDT technique employed above to determine if it also triggers Munc18-1 S241 phosphorylation in the LPP. Infusion of physostigmine (10 μM, 40 min) elicited a marked increase in slice levels of 2-AG ($P = 0.01$; Fig. 3*a*) but not other lipids (see Supplementary Fig. S2a); it also produced a reliable increase in SYN+ terminals with dense concentrations of pMunc18-1 in both LPP ($P = 0.009$; Fig. 3*b*) and S–C (see Supplementary Fig. S2b) fields. As predicted, physostigmine effects on both projections were dramatically reduced in slices prepared from Munc18-$1^{+/-}$ mice relative to those from wild types (LPP $P = 0.03$, Fig. 3*c*; see Supplementary Fig. S2c for CA1) although the mutation had no effect on the input/output (I/O) curve or paired-pulse facilitation in the LPP (see Supplementary Fig. S2d,e).

A recent study showed that the locally synthesized neurosteroid pregnenolone reduces both CB_1R signaling through ERK1/2 and neurotransmitter release suppression normally mediated by the ECB receptor (Vallee et al. 2014). We tested for this effect in hippocampus beginning with the pronounced fEPSP depression produced by CB_1R activation in the S–C system: treatment with 10 μM pregnenolone prevented the synaptic response depression elicited by WIN ($P = 0.0001$; Fig. 3*d*). Pregnenolone was similarly effective in the LPP where it blocked actions of physostigmine on presynaptic pMunc18-1 immunoreactivity ($P = 0.01$; Fig. 3*e*) and synaptic transmission ($P = 0.03$; Fig. 3*f*).

These findings point to the conclusion that the pregnenolone/CB_1R/Munc18-1 system, as found in the S–C projections, is present in the LPP although it is not engaged by either the CB_1R agonist WIN or repetitive afferent activity. There remains the possibility, however, that it is activated by the short high-frequency gamma trains used to induce *lpp*LTP and participates in subsequent stabilization of the potentiated state of LPP terminals. We conducted multiple tests of this argument. Pregnenolone at the concentration (10 μM) that eliminates physostigmine effects on transmission and pMunc18-1 immunoreactivity in CA1 had no detectable effect on *lpp*LTP induced by near threshold stimulation (Fig. 3*g*). Conventional stimulation trains failed to influence Munc18-1 phosphorylation in LPP terminals (Fig. 3*h*) and induction of *lpp*LTP was fully intact in Munc18-$1^{+/-}$ mice (Fig. 3*i*). Considered together with evidence that *lpp*LTP is both 2-AG and CB_1R-dependent (e.g., blocked by CB_1R antagonists AM215 and SR141716A, absent in CB_1R KOs, and augmented by increases in 2-AG) (Wang et al. 2016), the present results suggest that potentiation in the LPP involves a second CB_1R signaling pathway that has not been evaluated in work using physiological activation of hippocampal synapses.

Finally, the results obtained with pregnenolone afforded a means for testing if increases in 2-AG content produced by physostigmine promote *lpp*LTP in the absence of the response suppression associated with Munc18-1 phosphorylation. We tested this intriguing point and found that physostigmine more than doubled the magnitude of *lpp*LTP induced by threshold level stimulation ($P = 0.012$; Fig. 3*j*). This result is consistent with our earlier observation that reducing 2-AG breakdown, and thereby increasing hippocampal slice 2-AG levels, with the monoacylglycerol lipase (MGL) inhibitor JZL184 similarly augments *lpp*LTP (Wang et al. 2016).

CB_1R Signaling in LPP Terminals

Prior results showed that *lpp*LTP is blocked by presynaptic actions of latrunculin A (Wang et al. 2016), a toxin that selectively blocks the assembly of actin filaments. This raises the possibility that the CB_1R promotes *lpp*LTP via actions on actin regulatory signaling, an idea in alignment with evidence that CB_1R initiates actin reorganization in dissociated cells (Roland et al. 2014; Njoo et al. 2015) and rapidly (~2 min) activates both FAK and the small GTPase RhoA in N18TG2 neuroblastoma

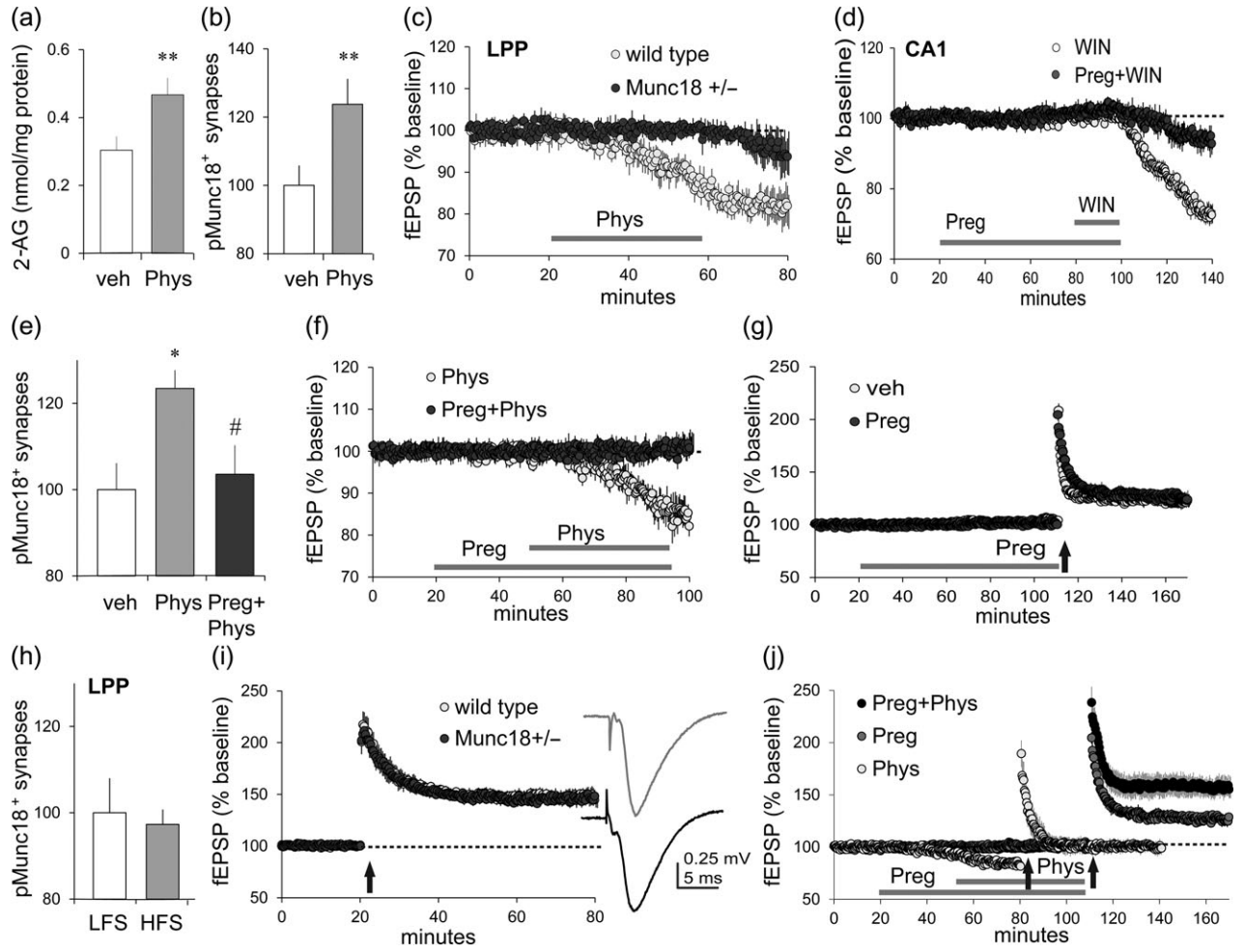

Figure 3. Biased CB_1R signaling to Munc18-1 is present in the LPP and modulated by pregnenolone. (*a–c*) Treatment of acute hippocampal slices with physostigmine (Phys; 10μM) (*a*) increased 2-AG content (nmol/mg protein) in hippocampus ($P = 0.01$, $t_{(17)} = 2.49$, 1-tail *t*-test; veh $n = 9$, Phys $n = 10$), (*b*) increased numbers of SYN immunopositive (+) terminal boutons enriched in pMunc18-1 S241 in the LPP field, as determined by FDT ($P = 0.009$, $t_{(22)} = 2.51$, 1-tail *t*-test; $n = 12$ ea), and (*c*) depressed LPP synaptic responses (fEPSPs) in slices from wild type mice but not from Munc18-1 heterozygotes ($Munc18^{+/-}$) ($P = 0.03$, $t_{(10)} = 2.54$; $n = 6$ ea). (*d*) Pregnenolone (Preg, 10 μM) blocked the otherwise robust suppression of field CA1 S–C responses achieved with WIN infusion ($P = 0.0001$, $t_{(9)} = 6.47$; WIN $n = 7$, Preg + WIN $n = 4$; WIN infused 50 min, Preg infused 80 min). (*e–g*) Pregnenolone (*e*) blocked physostigmine-induced increases in SYN+ boutons enriched in pMunc18-1 in the LPP field ($P = 0.01$, $F_{2,33} = 4.91$, 1-way ANOVA; with Bonferroni's post-test, veh vs. phys: $P < 0.05$, phys vs. preg+phys: $P < 0.05$; $n = 12$ ea) and (*f*) blocked suppression of LPP fEPSPs otherwise achieved by infusion of physostigmine ($P = 0.03$, $t_{(10)} = 2.54$; Phys $n = 7$, Phys+Preg: $n = 6$), but (*g*) did not impair *lpp*LTP achieved with near threshold HFS ($P = 0.33$, $t_{(10)} = 1.02$; $n = 6$ ea). (*h*) HFS, relative to LFS, had no effect on pMunc18-1 S241 in LPP terminals ($P = 0.77$, $t_{(17)} = 0.30$; LFS $n = 10$, HFS $n = 9$). (*i*) *lpp*LTP was comparable in wild type and Munc18-1 heterozygotes in response to conventional suprathreshold (HFS vs. LFS) ($P = 0.80$, $t_{(14)} = 0.26$; wild types $n = 7$, $Munc18\text{-}1^{+/-}$ $n = 9$); traces at right show representative fEPSPs for wild types (gray) and Munc18-1 hets (black) during the baseline period. (*j*) Physostigmine alone depressed LPP synaptic responses; under these conditions, HFS caused a small *lpp*LTP effect. Pregnenolone blocked the depressive effect of physostigmine on baseline LPP responses and uncovered a facilitatory action of the latter on *lpp*LTP in experiments using near threshold HFS ($P = 0.0015$, $F_{2,18} = 9.98$, 1-way ANOVA; Bonferroni's post-test, preg vs. phys: $P < 0.05$, phys vs. preg + phys: $P < 0.01$; preg: phys $n = 6$, preg + phys $n = 7$). Electrophysiological results are from field recordings; HFS applied at upward arrows. $^{*}P < 0.05$ versus veh, $^{\#}P < 0.05$ versus physostigmine; 2-tail *t*-test unless specified.

cells (Dalton et al. 2013). FAK is a non-receptor tyrosine kinase that mediates integrin effects on the actin cytoskeleton throughout the body (Fabry et al. 2011). Other experiments found that CB_1R acting through FAK initiates actin remodeling in pancreatic cells resulting in enhanced insulin release (Malenczyk et al. 2013). Accordingly, we used FDT to test if WIN activates FAK, via Y397 phosphorylation, in LPP terminals (Fig. 4*a*).

WIN produced a pronounced rightward skew in the immunofluorescence intensity-frequency distribution for pFAK Y397 co-localized with SYN ($P < 0.0001$; Fig. 4*b*). RhoA and its downstream effector, ROCK2, represent a primary route whereby FAK signals to actin (Chen et al. 2000; DeMali et al. 2003; Costa et al. 2013). In the LPP terminal field, WIN increased levels of pROCK S1366 (Chuang et al. 2012) co-localized with SYN ($P < 0.0001$; Fig. 4*c*) but not with the postsynaptic density marker PSD-95 ($P = 0.74$; Fig. 4*d*). In the same hippocampal slices, WIN increased presynaptic pROCK levels in CA1 but this effect was substantially smaller than that in the LPP. We quantified the regional difference by converting the data into cumulative probability curves and then subtracting the WIN-treatment values at each density bin for each slice from the mean curve for the vehicle group. The rightward shift in pROCK immunolabeling produced by WIN was over 2-fold greater in the LPP than in CA1 ($P < 0.0001$, $F_{17,23} = 6.105$, 2-way ANOVA). In all, the CB_1R agonist WIN had a much greater effect on Munc18-1

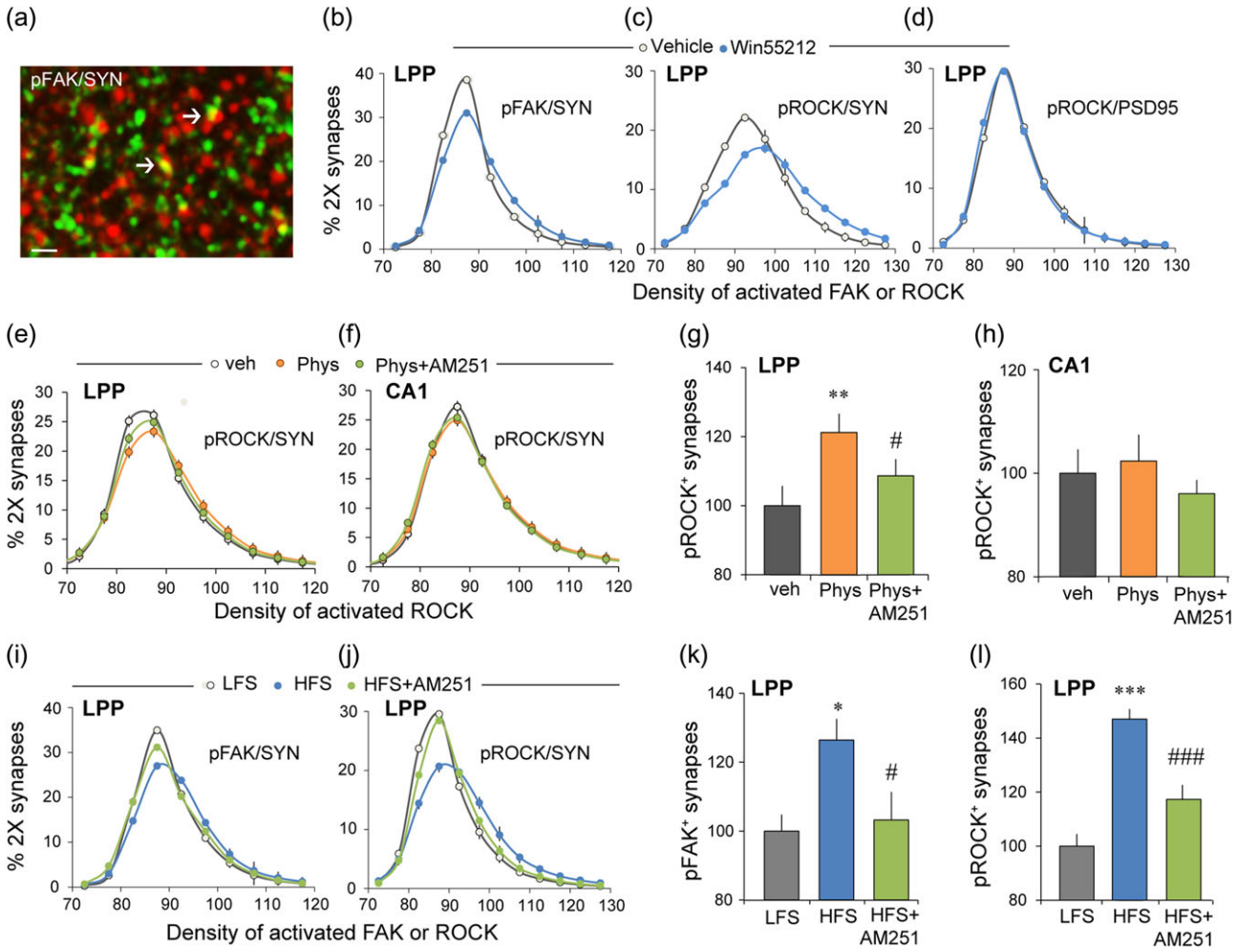

Figure 4. The CB_1R initiates actin regulatory signaling in LPP terminals. (*a–d*) Hippocampal slices were treated with CB_1R agonist WIN (5 μM, 30 min) or vehicle and harvested for FDT analysis of pROCK2 and pFAK immunoreactivities. (*a*) Deconvolved image shows immunofluorescent localization of pFAK (red) and SYN (green): yellow indicates double labeling (arrows) (bar = 10 μm). (*b*) WIN produced a rightward skew in the fluorescence intensity-frequency distribution curve (means ± SEM) for pFAK co-localized with SYN (veh = 10, WIN = 11 slices; 2-way ANOVA, $P < 0.0001$, $F_{21,396} = 8.65$). (*c*) Comparable results were obtained for presynaptic pROCK (2-way ANOVA, $P < 0.0001$, $F_{19,300} = 12.81$; veh = 9, WIN = 10 slices). (*d*) WIN did not affect the fluorescence intensity for pROCK co-localized with postsynaptic marker PSD-95 (2-way ANOVA, $P = 0.74$, $F_{21,396} = 0.78$; $n = 10$ ea). (*e–h*) Hippocampal slices were treated with 10 μM physostigmine (Phys) or vehicle for 60 min and then harvested for FDT analysis of pROCK2 in S–C and LPP terminals. (*e* and *f*) Physostigmine caused a right shift in the intensity-frequency distribution of presynaptic (SYN co-localized) pROCK that was reduced by AM251 in LPP terminals (*e*; 2-way ANOVA, $P < 0.0001$, $F_{38,855} = 3.40$); this effect was not present in CA1 (*f*; 2-way ANOVA, $P = 0.59$, $F_{38,855} = 0.93$). (*g* and *h*) Percent SYN+ terminals containing dense pROCK immunoreactivity (≥100 units) normalized to the value for control (veh) slices. Physostigmine increased densely pROCK+ terminals and this was blocked by AM251 for the LPP (*g*; $P = 0.0015$, $F_{2,47} = 5.86$, 1-way ANOVA; Bonferroni's post-test, veh vs. Phys: $P < 0.01$, Phys vs. Phys+AM251: $P < 0.05$, $n = 16$ ea.) but not in CA1 (*h*; $P = 0.57$, $F_{2,47} = 0.56$, 1-way ANOVA; $n = 16$ ea). (*i–l*) LTP-inducing HFS or baseline, LFS was delivered to the LPP and slices harvested 3 min later for immunofluorescence. (*i*) HFS caused a rightward shift in the intensity-frequency distribution of SYN co-localized pFAK and AM251 reduced this effect (2-way ANOVA, $P < 0.0001$, $F_{42,567} = 33.56$). (*j*) Comparable results were obtained for pROCK (2-way ANOVA, $P < 0.0001$, $F_{421,239} = 12.31$). (*k* and *l*) Percent of SYN+ terminals containing dense immunofluorescence (≥100 units) for pFAK (*k*) or pROCK (*l*) normalized to the value for control (LFS) slices. HFS increased numbers of such densely labeled terminals for both antigens and this was blocked by AM251 in both cases (for pFAK $P = 0.017$, $F_{2,28} = 4.76$; post-test: LFS vs. HFS: $P < 0.05$; HFS vs. HFS+AM251: $P < 0.05$; $n = 9–10$ slices/group; for pROCK $P < 0.0001$, $F_{2,61} = 26.92$; post-test: LFS vs. HFS: $P < 0.001$; HFS vs. HFS+AM251: $P < 0.001$, $n = 20–21$ slices/group; 1-way ANOVA and Bonferroni's post-test for both). $^{*}P < 0.05$, $^{**}P < 0.01$ versus veh or LFS; $^{\#}P < 0.05$, $^{\#\#\#}P < 0.001$ versus Phys or HFS.

phosphorylation in CA1 than in the LPP (Fig. 1*i*) and a much greater effect on markers of actin signaling in the LPP than in CA1. We conclude from this that the CB_1R response to WIN is biased toward different signaling streams in the 2 projections.

We further tested if CB_1R signaling to ROCK is more prominent in the LPP than in CA1 using physostigmine to elevate 2-AG levels and signaling. Physostigmine produced a reliable increase in presynaptic pROCK (i.e., a right shift in the density frequency distribution for SYN co-localized pROCK) in the LPP that was blocked by CB_1R antagonism ($P < 0.0001$; Fig. 4*e*) but had no reliable effect on presynaptic pROCK levels in CA1 of the same hippocampal slices ($P = 0.59$; Fig. 4*f*). A similar pattern of results was obtained in an analysis of the most densely pROCK immunoreactive terminal boutons (Fig. 4 *g*,*h*).

Collectively, these results describe a CB_1R-FAK-ROCK route by which 2-AG generated and released during high-frequency stimulation (HFS) could facilitate presynaptic cytoskeletal changes required for production of stable *lpp*LTP. In accord with this proposal, high-frequency bursts of LPP stimulation caused a rightward shift in the density frequency distribution of presynaptic pFAK in slices harvested 2 min after stimulation. The effect was blocked by AM251 at the concentration that

blocks *lpp*LTP ($P < 0.0001$; Fig. 4*i*,*k*). Similar CB_1R-dependent effects of HFS were obtained for pROCK (Fig. 4*j*,*l*). Finally, perfusion with FAK antagonist Y15 (40 μM) or ROCK inhibitor H1152 (0.1 μM) disrupted *lpp*LTP without affecting baseline responses (veh vs. Y15:70.8 ± 2.3% vs. 26.2 ± 5.1%, $P < 0.0001$, $t_{(10)} = 9.53$; veh vs. H1152:59.8 ± 8.6% vs. 25.5 ± 3.9%, $P = 0.0047$, $t_{(10)} = 3.62$; $n = 6$ ea, 2-tail *t*-test).

Together, these results describe a second CB_1R signaling pathway in LPP terminals that, unlike the ERK1/2-Munc18-1 route, is directly involved in the production of *lpp*LTP.

β1 Integrins are Critical for *lpp*LPP

An important question raised by the above results is why activation of FAK and ROCK by pharmacological CB_1R stimulation, augmented *lpp*LTP but did not by itself induce potentiation. One possibility is that electophysiological stimulation of the LPP engages elements that are not downstream from CB_1R activation but nonetheless are required for shifting LPP terminals into the enhanced release state. We tested if integrin class adhesion proteins, which co-operate with CB_1R in actin regulatory signaling in cultured cells (Dalton et al. 2013), fill this critical role. Integrins are dimeric transmembrane adhesion receptors for extracellular matrix and cell surface proteins that are expressed throughout the brain by neurons and glia (Park and Goda 2016). In hippocampus the majority of integrins contain the β1 subunit (Pinkstaff et al. 1999) and β1 integrins have been localized to both pre- and postsynaptic compartments (Schuster et al. 2001; Park and Goda 2016). We previously demonstrated that, in hippocampal slices, infusion of β1 neutralizing antisera disrupts activity-induced actin polymerization and LTP in field CA1 (Kramar et al. 2006). Here, we tested if similar treatments influence potentiation in the LPP. Treatment with anti-β1 had no effect on baseline LPP responses but caused a near complete suppression of *lpp*LTP ($P < 0.0001$; Fig. 5*a*). In contrast, neutralizing anti-αV integrin left potentiation intact ($P = 0.43$; Fig. 5*b*). We then assessed *lpp*LTP in slices from conditional β1 KO mice. For these studies, mice with floxed β1 exon 3 (B6;129-Itgb1tm1Efu/J strain) were crossed with CaMKIIα-Cre mice (B6.Cg-Tg(Camk2a-cre)T29-firstl/J) to generate KOs with β1 expression depressed in excitatory hippocampal neurons beginning in the third week of life (Wang et al. 2016a). The LPP I/O curve in β1 KOs was slightly depressed relative to wild types but this effect did not approach statistical significance ($P = 0.17$; Fig. 5*c*). Waveform characteristics were also comparable between KOs and wild types (Fig. 5*c*, inset); quantitatively, the mean time constants for the rising and decay phases of the fEPSP were not detectably different. Despite seemingly normal fEPSPs, the β1 KOs had severely impaired *lpp*LPP ($P = 0.005$; Fig. 5*d*).

A major subset of β1 family integrins bind an Arg-Gly-Asp (RGD) consensus sequence in their matrix ligands (Humphries et al. 2006). Snake toxin "disintegrins," including echistatin, contain an RGD mimetic sequence that blocks this integrin subgroup. We confirmed that infusion of echistatin blocks the stabilization of postsynaptic LTP in field CA1 ($P = 0.0012$; Fig. 5*e*), as previously reported (Chun et al. 2001), and then tested for effects on *lpp*LTP. Echistatin had no detectable influence on *lpp*LTP measured 55–60 min postinduction ($P = 0.628$; Fig. 5*f*). We compared the results obtained with the various integrin manipulations by normalizing the percent *lpp*LTP per experimental slice to the mean value for yoked vehicle cases. There was a highly significant group effect for treatment ($P = 0.0003$; Fig. 5*g*) with measures of potentiation from the anti-β1 group being lower than those from control, anti-αV, or echistatin groups (***$P < 0.001$, **$P < 0.01$). The anti-αV and echistatin

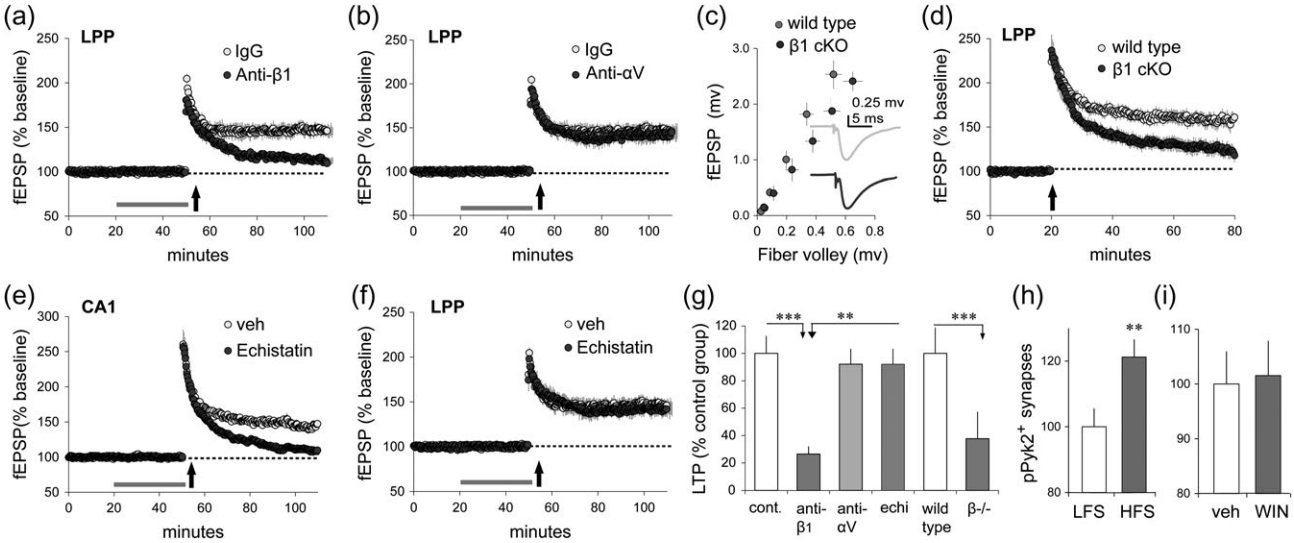

Figure 5. Production of *lpp*LTP is β1-integrin dependent. (*a*–*g*) Hippocampal slices received stimulation of LPP or S–C projections ("e" only) to assess the effects of pharmacological or genetic manipulation of integrins on plasticity. (*a*) Infusion of neutralizing anti-β1-integrin blocked stabilization of *lpp*LTP while the control immunoglobulin (IgG) had no effect ($P < 0.0001$, $t_{(11)} = 7.21$; IgG $n = 6$, anti-β1 $n = 7$). (*b*) Neutralizing anti-αV integrin did not affect *lpp*LTP ($P = 0.43$, $t_{(9)} = 0.83$; IgG $n = 6$, anti-αV $n = 5$). (*c*) The fiber volley amplitude versus fEPSP amplitude relationship (I/O curve) for wild types and conditional β1-integrin KO mice were comparable (2-way ANOVA, $P = 0.17$, $F_{5,65} = 1.63$; wild type $n = 10$, β1 KO $n = 13$); inset shows representative fEPSP traces. (*d*) High-frequency LPP stimulation induced comparable initial potentiation in wild type and β1 KO mice but the level of potentiation then fell steadily toward baseline in KOs only ($P = 0.005$, $t_{(21)} = 3.18$; wild type $n = 10$, β1 KO $n = 13$). (*e* and *f*) The disintegrin echistatin (10 μM) blocked LTP in CA1 (*e*; $P = 0.0012$, $t_{(9)} = 4.63$; veh $n = 4$, echistatin $n = 7$) but had no effect on *lpp*LTP (*f*; $P = 0.628$, $t_{(8)} = 0.504$; veh $n = 6$, echistatin $n = 7$). (*g*) Summary graph shows the magnitude of *lpp*LTP after integrin-targeted manipulations % potentiation vs. baseline for individual slices, normalized to paired control group means; $P = 0.0003$, $F_{3,17} = 11.19$, 1-way ANOVA and Bonferroni's Multiple Comparison Test. The percent of SYN+ boutons associated with dense pPyk2 immunolabeling (≥92 intensity) in the LPP field normalized to the value for control slices: (*h*) HFS produced a robust increase relative to LFS ($P = 0.012$, $t_{(22)} = 2.74$; $n = 12$ ea) while (*i*) WIN had no effect relative to vehicle ($P = 0.87$, $t_{(22)} = 0.17$; veh $n = 13$, WIN $n = 11$). **$P < 0.01$, ***$P < 0.001$; 2-tail *t*-test unless otherwise specified.

treatment groups exhibited potentiation that did not differ from each other or from controls.

Next, we tested for integrin signaling that is activated by HFS but not by pharmacological activation of the CB_1Rs. A likely additional factor is proline-rich tyrosine kinase-2 (Pyk2), a second integrin-associated tyrosine kinase that produces downstream effects beyond those targeted by the homologous FAK (Girault et al. 1999). Physiological stimulation increased the number of terminals with high density pPyk2 immunolabeling ($P = 0.012$; Fig. 5*h*). In contrast, WIN did not affect the percentage of LPP terminals with dense concentrations of pPyk2 ($P = 0.87$; Fig. 5*i*). These findings point to a hypothesis in which high-frequency LPP stimulation activates β1 family integrins and their signaling to 2 associated tyrosine kinases, one of which (FAK) is targeted by 2-AG signaling through the CB_1R. This co-operative signaling then produces the presynaptic cytoskeletal changes required for lasting increases in transmitter release.

Activation of synaptic integrin signaling by physiological activity is reported to involve ligands generated from the extracellular matrix by metalloproteinases (MMPs), and by MMP9 in particular (Nagy et al. 2006). We tested for involvement of this mechanism in the LPP and found that perfusion of the broad MMP inhibitor GM 6001 (25 μM) produced a significant impairment of *lpp*LTP (veh 70.1 ± 4.7%; GM6000 40.9 ± 3.6%; $P = 0.0006$, $t_{(10)} = 4.94$, 2-tail *t*-test, $n = 6$ ea) without effect on baseline responses.

LPP-Dependent Learning Induces *lpp*LTP

Lateral entorhinal cortex neurons that generate the LPP receive dense input from the adjacent olfactory (piriform) cortex and neocortical associational regions. Prior studies confirmed that the LPP is critical for learning two-odor discriminations (Staubli et al. 1984; Otto et al. 1991) and, more recently, that AM251 blocks this encoding whereas suppression of 2-AG degradation enhances it (Wang et al. 2016). We accordingly used the 2-odor paradigm to test if learning elicits signaling associated with the production of *lpp*LTP. Rats were trained on a series of ten novel discriminations over successive days until they showed a strong preference for the positive cue in trials 6–10. Past work showed that such learning results in long-term memory (Larson et al. 1995). A novel odor pair was presented on the test day. Animals were euthanized immediately after the 10th training trial and sections through rostral hippocampus (Fig. 6*a*) were processed for dual immunostaining (SYN and pROCK) and FDT analysis: ~400 000 SYN+ structures fitting the size and eccentricity constraints of synapses were reconstructed in 3D from image z-stacks in the LPP field within the outer molecular layer of the DG. The data were expressed as percent of all bouton-sized SYN clusters for each of a series of increasing pROCK density bins. The immunofluorescence intensity-frequency distribution for SYN co-localized pROCK was skewed to the right for rats trained in the olfactory discrimination relative to untrained controls ($P < 0.0001$; Fig. 6*b*), indicating that the learning group had greater concentrations of pROCK in LPP terminals (LPP afferents comprise over 80% of the innervation in this lamina). Increases in pROCK immunolabeling produced by odor learning were eliminated by AM251 (1 mg/kg) given 1 h before training ($P < 0.0001$; Fig. 6*b*).

There was a small but significant difference in the total number of SYN clusters in the AM251 group relative to the odor learning plus vehicle (–5.9%, $P < 0.01$, *t*-test) or control (–6.7%, $P < 0.04$) animals. To minimize any effects of this, we recalculated the above data for each pROCK density bin for each animal as a percentage of all double-labeled contacts for that animal, with the results expressed as a cumulative probability function. The mean curve for the learning plus vehicle group was clearly displaced to the right relative to that for the learning plus AM251 or for control rats (RM-ANOVA: $P < 0.0001$ in each case); the results for the latter 2 groups were superimposed on each other (Fig. 6*c*). A bootstrap analysis (Stein 1989) using randomly selected pairs of animals (1000 pairs per run; 15 runs) confirmed that the summed deviations between curves were much greater for learning versus control groups (20×) than for the learning + AM251 versus control groups (3×) ($P < 0.0001$, *t*-test).

Discussion

The present studies provide a first detailed description of the mechanisms underlying a novel form of LTP in a primary cortical input to hippocampus. Given that this projection conveys semantic ("what is it") information to hippocampus (Eichenbaum et al. 2012; Reagh and Yassa 2014), the findings are of basic importance to

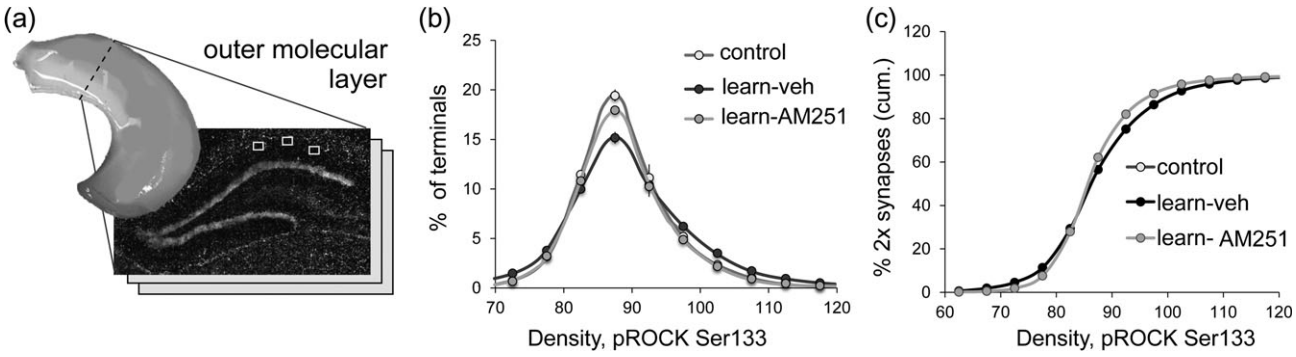

Figure 6. Learning of cues conveyed by the LPP produces synaptic effects associated with *lpp*LTP. (*a*) Location of DG molecular layer sample zones for measures of SYN co-localized pROCK. (*b*) Phospho-ROCK labeling co-localized with SYN is described as a percent of the total population of bouton-sized SYN clusters for each of an ascending series of pROCK density bins. The resultant distribution (means ± SEMs) is right-skewed in vehicle treated rats after learning a novel odor pair (learn-veh, $n = 16$) relative to the transport "control" group ($n = 17$) ($P < 0.0001$, $F_{24,720} = 5.14$, 2-way ANOVA, control vs. learn-veh); this effect was blocked by AM251 ($n = 8$) ($P < 0.0001$, $F_{24,528} = 2.61$, 2-way ANOVA, learn-veh vs. learn-AM251). (*c*) The data for pROCK density bins for each animal were calculated as % of all double-labeled synapses for that animal (rather than as % total SYN positive boutons) and the results plotted as cumulative probability functions. The mean (±SEMs) curve for the learning-veh group was again displaced from those for the control group ($P < 0.0001$; $F_{24,696} = 5.020$, 2-way RM-ANOVA) and learning animals treated with AM251 ($P < 0.0001$; $F_{24,528} = 4.481$, 2-way RM-ANOVA). The cumulative probability curves for the latter 2 groups (control and learning-AM251) could not be distinguished.

the development of neurobiologically based theories of episodic memory. The substrates for *lpp*LTP include a repurposing of elements utilized in conventional, postsynaptic potentiation, as described for the intensively studied S–C projection to CA1, supplemented with novel features. Both forms of potentiation are induced postsynaptically via NMDARs and increased calcium levels (Collingridge et al. 1983; Lynch et al. 1983; Granger and Nicoll 2014), and both require activation of β1 integrins and their downstream effector ROCK (Chan et al. 2006; Kramar et al. 2006; Rex et al. 2009). Integrins are a primary membrane regulator of the actin cytoskeleton (DeMali et al. 2003) and their prominent role in both types of plasticity suggests that activity-induced structural changes constitute a shared endpoint. Potentiation of S–C synapses in field CA1 entails integrin-driven assembly of stable actin networks in dendritic spines and an associated shift in spine/synapse morphology (Kramar et al. 2006; Chen et al. 2007; Rudy 2015). Morphometric studies have yet to be performed for *lpp*LTP but results obtained with the toxin latrunculin A, which selectively blocks actin filament assembly, confirm that in this system the cytoskeletal reorganization is located presynaptically (Wang et al. 2016). Thus, integrin regulation of the cytoskeleton, via signaling common to cell adhesion junctions throughout the body, underlies both forms of potentiation but in the case of *lpp*LTP these processes are active on the presynaptic side. This specialized feature of the LPP results in a new form of LTP.

Earlier work showed that LTP induction in the LPP requires stimulation of mGluR5 receptors, something that was not the case for field CA1 or the medial perforant path (Wang et al. 2016). The mGluR5 receptor forms a postsynaptic signalosome with the scaffolding protein Homer and the 2-AG synthesizing enzyme diacylglycerol lipase-α (DAGL-α) (Jung et al. 2012). Activation of this unit results in de novo 2-AG production and retrograde signaling to presynaptic CB_1Rs, 2 events shown to be essential for *lpp*LTP (Wang et al. 2016). The present results establish that this dependency is not due to canonical CB_1R signaling, which produces depression of transmitter release (Castillo et al. 2012) at sites throughout the brain. Instead, the critical contribution of CB_1Rs to *lpp*LTP involves activation of the integrin-associated kinase FAK and its downstream effector ROCK with high-frequency afferent activity. We found that the CB_1R inverse agonist AM251 prevented such activation, whereas the CB_1R agonist WIN mimicked it and also lowered the threshold for induction of *lpp*LTP. Conversely, the release depression function of the CB_1R was poorly developed in the LPP and not involved in the potentiation effect. ECB-mediated release suppression is reportedly sensitive to locally synthesized pregnenolone (Vallee et al. 2014) and involves phosphorylation of the vesicular protein Munc18-1 (Schmitz et al. 2016). These effects were evident in S–C projections to CA1 but not in the LPP. Specifically, treatment with CB_1R agonist WIN increased phosphorylation of Munc18-1 and caused a Munc18-1 dependent, pregnenolone-sensitive depression of synaptic responses in field CA1. In contrast, neither pregnenolone nor reductions in Munc18-1 expression affected *lpp*LTP. We propose that a shift in the bias of CB_1R signaling away from the Munc18-1 pathway and toward facilitation of the ROCK/FAK, integrin signaling cascade constitutes a projection system-specific specialization that enables the thus far singular form of LTP found in the LPP (Fig. 7).

There is precedence for both ligand- and cell-type-specific differences in CB_1R signaling (Varga et al. 2008; Laprairie et al. 2014). Ligands for CB_1R, including the ECBs, synthetic cannabinoids such as WIN and phytocannabinoids such as Δ^9-tetrahydrocannabinol, all bind different residues on the receptor. This has been

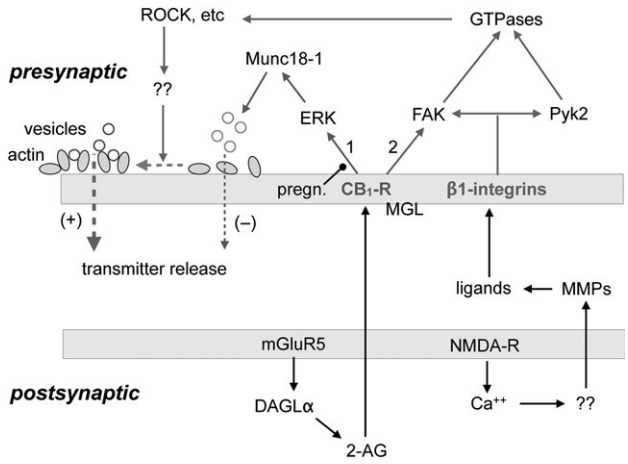

Figure 7. Proposed substrates for LTP in the LPP. Glutamate released during bursts of high-frequency gamma activity binds to mGluR5 receptors resulting in activation of the enzyme DAGL-α and the synthesis of 2-AG. The ECB diffuses from the postsynaptic compartment to CB_1Rs located on LPP terminals where it is degraded by MGL. CB_1Rs initiate 2 signaling cascades. The first (#1) which is depressed by pregnenolone (pregn), engages ERK leading to phosphorylation and degradation of the vesicle protein Munc18-1. This depresses vesicle-membrane fusion and glutamate release. The second (#2) CB_1R pathway stimulates integrin-associated FAK, which targets small GTPases (RhoA) and ROCK. CB_1R signaling is biased toward pathway #1 in the S–C projection in CA1 but toward pathway #2 in the LPP. Related to this, the Munc18-1 route does not contribute to *lpp*LTP while the FAK route is necessary but not sufficient for production of *lpp*LTP. Expression of this atypical LPP potentiation also requires activation of a subclass (nonRGD) of β1 integrins by high-frequency afferent activity. It is proposed that ligands for these presynaptic integrins are generated by NMDAR activation, associated increases in postsynaptic calcium, and the release of unspecified factors ("??") that activate extracellular MMPs. The latter generate matrix protein fragments that bind to the integrins and contribute to their activation. Integrins, in conjunction with CB_1R, signal to FAK and separately engage a second, homologous kinase (Pyk2). The tyrosine kinases then activate small GTPases and their downstream effectors (ROCK, etc.) along with other actin signaling events ("??") leading to reorganization of the presynaptic cytoskeleton (dashed horizontal line). This results in enhanced glutamate release probability by improved vesicle docking.

suggested to give rise to ligand-specific conformational changes in CB_1R leading to activation of different downstream signaling pathways (Georgieva et al. 2008; Varga et al. 2008; Hudson et al. 2010). Moreover, the functional selectivity of a given ligand can be cell-type-specific (Bosier et al. 2010). In line with these observations, we found cell-type-specific differences in CB_1R-mediated responses to a given ligand (e.g., WIN depressed baseline transmission in CA1 but not in the LPP) and differences in CB_1R response to different ligands for a given cell-type (e.g., the robust 2-AG signaling induced by physostigmine increased LPP pMunc18-1 and suppressed LPP baseline responses whereas WIN elicited neither effect).

The evidence for projection-specific differences in CB_1R signaling gives rise to the prediction that modulation of synaptic transmission by ECBs during behaviorally relevant patterns of synaptic activity, a topic that has received surprisingly little attention, will differ between the S–C and LPP systems. Tests confirmed that stimulation in the low-frequency gamma (40 Hz) range, selected to simulate the activity in fields CA3 and CA1 during exploration (Colgin 2015), engages CB_1Rs to depress synaptic responses generated by the S–C, but not LPP, projections. Thus, the projection-specific bias in CB_1R function is likely to differentially influence throughput across the nodes of the primary hippocampal network. An interesting issue for future research concerns the extent to which the contribution of ECBs to synaptic function is frequency-tuned and differs

across hippocampal rhythms (beta, gamma, theta, etc.) associated with various behaviors.

Prior work showed that blocking or enhancing the production of 2-AG produces corresponding effects on both the magnitude of *lpp*LTP and the encoding of olfactory cues carried to hippocampus by the LPP system (Wang et al. 2016). The present experiments demonstrate that olfactory discrimination learning elicits evidence for potentiation in the form of increased presynaptic pROCK within the LPP. Questions thus arise about the functional significance of using a specialized form of plasticity to encode the semantic ("what") information carried by the LPP. One possibility is that the specialization helps to maintain cue identity through downstream hippocampal processing. The novel *lpp*LTP effect changes the frequency facilitation characteristics of the LPP, as evidenced by paired-pulse measurements, something that would be expected to alter the spiking response of granule cells to patterned input. This would serve to differentiate the DG outputs produced by learned versus unlearned cues and help maintain cue identity through downstream processing. It would also further distinguish the response of granule cells to input arriving over the LPP from those elicited by the subjacent medial perforant path (spatial information). Related to this, insertion of a 2-AG step in the mechanisms for encoding opens the way for modulation of *lpp*LTP by afferents arising from sites other than entorhinal cortex. Cholinergic inputs from the medial septum and diagonal bands are of particular interest in this regard because enhancing constitutive transmission in this projection elevates 2-AG levels and related CB_1R signaling in terminals. We used this effect to confirm that the Munc18-1 release suppression system is present in the LPP although not engaged by WIN or afferent stimulation. The studies also demonstrated that increasing cholinergic transmission has a strong positive effect on the production *lpp*LTP, particularly when release suppression machinery is blocked with pregnenolone. It is, therefore, possible that particular patterns of firing by septal afferents or levels of pregnenolone synthesis promote the presynaptic LTP in the LPP while depressing the postsynaptic variant found in the medial perforant path. Such a mechanism could be of value when semantic information has a higher priority than spatial data.

Finally, the present evidence for biased CB_1R signaling has significant implications for hypotheses about how marijuana influences cognition. The Δ^9-tetrahydrocannabinol component of cannabis is an agonist for CB_1Rs and stimulates the production of pregnenolone (Vallee et al. 2014); results presented here indicate that the combination of CB_1R stimulation and high levels of pregnenolone will lower the requirements for robust *lpp*LTP and the encoding of near threshold cues. It is interesting regarding this possibility that marijuana promotes the formation of false memories in episodic memory tests (Riba et al. 2015). In all, the differential effects of CB_1R stimulation across the principal nodes of hippocampal circuitry are predicted to underlie a distortion of episodic memory with cannabis exposure that is due to enhanced plasticity in the LPP.

Supplementary Material

Supplementary material is available at *Cerebral Cortex* online.

Funding

National Institutes of Health (NS085709, P01NS045260, HD08949101 to G.L. and C.M.G.), (MH096847, MH108408, NS064079 to G.R.), and (DA012413, DA031387 to D.P.).

Notes

We thank Dr. Julie C. Lauterborn for assistance with immunofluorescence and Dr. Ken Mackie for providing CB_1R antisera. *Conflict of Interest*: The authors declare no competing financial interests.

References

Aggleton JP, Brown MW. 1999. Episodic memory, amnesia, and the hippocampal-anterior thalamic axis. Behav Brain Sci. 22: 425–444. discussion 444–489.

Amaral D, Lavenex P. 2007. Hippocampal Neuroanatomy. In: Andersen P, Morris RG, Amaral D, Bliss TV, O'Keefe J, editors. The hippocampus book. New York: Oxford University Press. p. 37–114.

Bock HH, Herz J. 2003. Reelin activates SRC family tyrosine kinases in neurons. Curr Biol. 13:18–26.

Bosier B, Muccioli GG, Hermans E, Lambert DM. 2010. Functionally selective cannabinoid receptor signalling: therapeutic implications and opportunities. Biochem Pharmacol. 80:1–12.

Castillo PE, Younts TJ, Chavez AE, Hashimotodani Y. 2012. Endocannabinoid signaling and synaptic function. Neuron. 76:70–81.

Chan CS, Weeber EJ, Zong L, Fuchs E, Sweatt JD, Davis RL. 2006. Beta 1-integrins are required for hippocampal AMPA receptor-dependent synaptic transmission, synaptic plasticity, and working memory. J Neurosci. 26:223–232.

Chen LM, Bailey D, Fernandez-Valle C. 2000. Association of beta 1 integrin with focal adhesion kinase and paxillin in differentiating Schwann cells. J Neurosci. 20:3776–3784.

Chen LY, Rex CS, Casale MS, Gall CM, Lynch G. 2007. Changes in synaptic morphology accompany actin signaling during LTP. J Neurosci. 27:5363–5372.

Christie BR, Abraham WC. 1994. Differential regulation of paired-pulse plasticity following LTP in the dentate gyrus. Neuroreport. 5:385–388.

Chuang HH, Yang CH, Tsay YG, Hsu CY, Tseng LM, Chang ZF, Lee HH. 2012. ROCKII Ser1366 phosphorylation reflects the activation status. Biochem J. 443:145–151.

Chun D, Gall CM, Bi X, Lynch G. 2001. Evidence that integrins contribute to multiple stages in the consolidation of long term potentiation in rat hippocampus. Neuroscience. 105: 815–829.

Colgin LL. 2015. Do slow and fast gamma rhythms correspond to distinct functional states in the hippocampal network? Brain Res. 1621:309–315.

Colgin LL, Kramar EA, Gall CM, Lynch G. 2003. Septal modulation of excitatory transmission in hippocampus. J Neurophysiol. 90:2358–2366.

Collingridge GL, Kehl SJ, McLennan H. 1983. Excitatory amino acids in synaptic transmission in the Schaffer collateral-commissural pathway of the rat hippocampus. J Physiol. 334:33–46.

Costa P, Scales TM, Ivaska J, Parsons M. 2013. Integrin-specific control of focal adhesion kinase and RhoA regulates membrane protrusion and invasion. PLoS One. 8:e74659.

Dalton GD, Peterson LJ, Howlett AC. 2013. CB(1) cannabinoid receptors promote maximal FAK catalytic activity by stimulating cooperative signaling between receptor tyrosine kinases and integrins in neuronal cells. Cell Signal. 25: 1665–1677.

DeMali KA, Wennerberg K, Burridge K. 2003. Integrin signaling to the actin cytoskeleton. Curr Opin Cell Biol. 15:572–582.

Diana MA, Marty A. 2004. Endocannabinoid-mediated short-term synaptic plasticity: depolarization-induced suppression of inhibition (DSI) and depolarization-induced suppression of excitation (DSE). Br J Pharmacol. 142:9–19.

Eichenbaum H. 2000. A cortical-hippocampal system for declarative memory. Nat Rev Neurosci. 1:41–50.

Eichenbaum H, Fortin NJ. 2005. Bridging the gap between brain and behavior: cognitive and neural mechanisms of episodic memory. J Exp Anal Behav. 84:619–629.

Eichenbaum H, Sauvage M, Fortin N, Komorowski R, Lipton P. 2012. Towards a functional organization of episodic memory in the medial temporal lobe. Neurosci Biobehav Rev. 36: 1597–1608.

Fabry B, Klemm AH, Kienle S, Schaffer TE, Goldmann WH. 2011. Focal adhesion kinase stabilizes the cytoskeleton. Biophys J. 101:2131–2138.

Georgieva T, Devanathan S, Stropova D, Park CK, Salamon Z, Tollin G, Hruby VJ, Roeske WR, Yamamura HI, Varga E. 2008. Unique agonist-bound cannabinoid CB1 receptor conformations indicate agonist specificity in signaling. Eur J Pharmacol. 581:19–29.

Girault J-A, Costa A, Dirkinderen P, Studler J-M, Toutant M. 1999. FAK and PYK2/CASβ in the nervous system: a link between neuronal activity, plasticity, and survival. Trnds Neurosci. 22:257–263.

Granger AJ, Nicoll RA. 2014. Expression mechanisms underlying long-term potentiation: a postsynaptic view, 10 years on. Philos Trans R Soc Lond B Biol Sci. 369:20130136.

Hudson BD, Hebert TE, Kelly ME. 2010. Ligand- and heterodimer-directed signaling of the CB(1) cannabinoid receptor. Mol Pharmacol. 77:1–9.

Humphries JD, Byron A, Humphries MJ. 2006. Integrin ligands at a glance. J Cell Sci. 119:3901–3903.

Jung KM, Astarita G, Zhu C, Wallace M, Mackie K, Piomelli D. 2007. A key role for diacylglycerol lipase-alpha in metabotropic glutamate receptor-dependent endocannabinoid mobilization. Mol Pharmacol. 72:612–621.

Jung KM, Sepers M, Henstridge CM, Lassalle O, Neuhofer D, Martin H, Ginger M, Frick A, DiPatrizio NV, Mackie K, et al. 2012. Uncoupling of the endocannabinoid signalling complex in a mouse model of fragile X syndrome. Nat Commun. 3:1080.

Katona I, Urban GM, Wallace M, Ledent C, Jung KM, Piomelli D, Mackie K, Freund TF. 2006. Molecular composition of the endocannabinoid system at glutamatergic synapses. J Neurosci. 26:5628–5637.

Kramar EA, Bernard JA, Gall CM, Lynch G. 2003. Integrins modulate fast excitatory transmission at hippocampal synapses. J Biol Chem. 278:10722–10730.

Kramar EA, Lin B, Rex CS, Gall CM, Lynch G. 2006. Integrin-driven actin polymerization consolidates long-term potentiation. Proc Natl Acad Sci USA. 103:5579–5584.

Laprairie RB, Bagher AM, Kelly ME, Dupre DJ, Denovan-Wright EM. 2014. Type 1 cannabinoid receptor ligands display functional selectivity in a cell culture model of striatal medium spiny projection neurons. J Biol Chem. 289: 24845–24862.

Larson J, Lieu T, Petchpradub V, LeDuc B, Ngo H, Rogers GA, Lynch G. 1995. Facilitation of olfactory learning by a modulator of AMPA receptors. J Neurosci. 15:8023–8030.

Lynch G, Kramar EA, Babayan AH, Rumbaugh G, Gall CM. 2013. Differences between synaptic plasticity thresholds result in new timing rules for maximizing long-term potentiation. Neuropharmacology. 64:27–36.

Lynch G, Larson J, Kelso S, Barrionuevo G, Schottler F. 1983. Intracellular injections of EGTA block induction of hippocampal long-term potentiation. Nature. 305:719–721.

Lynch G, Rex CS, Gall CM. 2007. LTP consolidation: substrates, explanatory power, and functional significance. Neuropharmacology. 52:12–23.

Malenczyk K, Jazurek M, Keimpema E, Silvestri C, Janikiewicz J, Mackie K, Di Marzo V, Redowicz MJ, Harkany T, Dobrzyn A. 2013. CB1 cannabinoid receptors couple to focal adhesion kinase to control insulin release. J Biol Chem. 288: 32685–32699.

Martens KM, Vonder Haar C, Hutsell BA, Hoane MR. 2013. The dig task: a simple scent discrimination reveals deficits following frontal brain damage. J Vis Exp. 4. doi:10.3791/50033.

Matyas F, Yanovsky Y, Mackie K, Kelsch W, Misgeld U, Freund TF. 2006. Subcellular localization of type 1 cannabinoid receptors in the rat basal ganglia. Neuroscience. 137: 337–361.

Mortillo S, Elste A, Ge Y, Patil SB, Hsiao K, Huntley GW, Davis RL, Benson DL. 2012. Compensatory redistribution of neuroligins and N-cadherin following deletion of synaptic beta1-integrin. J Comp Neurol. 520:2041–2052.

Nagy V, Bozdagi O, Matynia A, Balcerzyk M, Okulski P, Dzwonek J, Costa RM, Silva AJ, Kaczmarek L, Huntley GW. 2006. Matrix metalloproteinase-9 is required for hippocampal late-phase long-term potentiation and memory. J Neurosci. 26:1923–1934.

Njoo C, Agarwal N, Lutz B, Kuner R. 2015. The cannabinoid receptor CB1 interacts with the WAVE1 complex and plays a role in actin dynamics and structural plasticity in neurons. PLoS Biol. 13:e1002286.

Otto T, Schottler F, Staubli U, Eichenbaum H, Lynch G. 1991. Hippocampus and olfactory discrimination learning: effects of entorhinal cortex lesions on olfactory learning and memory in a successive-cue, go-no-go task. Behav Neurosci. 105: 111–119.

Park YK, Goda Y. 2016. Integrins in synapse regulation. Nat Rev Neurosci. 17:745–756.

Paton GS, Pertwee RG, Davies SN. 1998. Correlation between cannabinoid mediated effects on paired pulse depression and induction of long term potentiation in the rat hippocampal slice. Neuropharmacology. 37:1123–1130.

Pinkstaff JK, Detterich J, Lynch G, Gall C. 1999. Integrin subunit gene expression is regionally differentiated in adult brain. J Neurosci. 19:1541–1556.

Reagh ZM, Yassa MA. 2014. Object and spatial mnemonic interference differentially engage lateral and medial entorhinal cortex in humans. Proc Natl Acad Sci USA. 111:E4264–E4273.

Rex CS, Chen LY, Sharma A, Liu J, Babayan AH, Gall CM, Lynch G. 2009. Different Rho GTPase-dependent signaling pathways initiate sequential steps in the consolidation of long-term potentiation. J Cell Biol. 186:85–97.

Riba J, Valle M, Sampedro F, Rodriguez-Pujadas A, Martinez-Horta S, Kulisevsky J, Rodriguez-Fornells A. 2015. Telling true from false: cannabis users show increased susceptibility to false memories. Mol Psychiatry. 20:772–777.

Roland AB, Ricobaraza A, Carrel D, Jordan BM, Rico F, Simon A, Humbert-Claude M, Ferrier J, McFadden MH, Scheuring S, et al. 2014. Cannabinoid-induced actomyosin contractility shapes neuronal morphology and growth. Elife. 3:e03159.

Rudy JW. 2015. Actin dynamics and the evolution of the memory trace. Brain Res. 1621:17–28.

Salz DM, Tiganj Z, Khasnabish S, Kohley A, Sheehan D, Howard MW, Eichenbaum H. 2016. Time cells in hippocampal area CA3. J Neurosci. 36:7476–7484.

Schmitz SK, King C, Kortleven C, Huson V, Kroon T, Kevenaar JT, Schut D, Saarloos I, Hoetjes JP, de Wit H, et al. 2016. Presynaptic inhibition upon CB1 or mGlu2/3 receptor activation requires ERK/MAPK phosphorylation of Munc18-1. EMBO J. 35:1236–1250.

Schuster T, Krug M, Stalder M, Hackel N, Gerardy-Schahn R, Schachner M. 2001. Immunoelectron microscopic localization of the neural recognition molecules L1, NCAM, and its isoform NCAM180, the NCAM-associated polysialic acid, beta1 integrin and the extracellular matrix molecule tenascin-R in synapses of the adult rat hippocampus. J Neurobiol. 49:142–158.

Seese RR, Babayan AH, Katz AM, Cox CD, Lauterborn JC, Lynch G, Gall CM. 2012. LTP induction translocates cortactin at distant synapses in wild-type but not Fmr1 knock-out mice. J Neurosci. 32:7403–7413.

Seese RR, Chen LY, Cox CD, Schulz D, Babayan AH, Bunney WE, Henn FA, Gall CM, Lynch G. 2013. Synaptic abnormalities in the infralimbic cortex of a model of congenital depression. J Neurosci. 33:13441–13448.

Seese RR, Wang K, Yao YQ, Lynch G, Gall CM. 2014. Spaced training rescues memory and ERK1/2 signaling in fragile X syndrome model mice. Proc Natl Acad Sci USA. 111: 16907–16912.

Staubli U, Ivy G, Lynch G. 1984. Hippocampal denervation causes rapid forgetting of olfactory information in rats. Proc Natl Acad Sci USA. 81:5885–5887.

Stine R. 1989. An introduction to boostrap methods. Sociol Methods Res. 18:243–291.

Takahashi H, Arstikaitis P, Prasad T, Bartlett TE, Wang YT, Murphy TH, Craig AM. 2011. Postsynaptic TrkC and presynaptic PTPsigma function as a bidirectional excitatory synaptic organizing complex. Neuron. 69:287–303.

Trieu BH, Kramar EA, Cox CD, Jia Y, Wang W, Gall CM, Lynch G. 2015. Pronounced differences in signal processing and synaptic plasticity between piriform-hippocampal network stages: a prominent role for adenosine. J Physiol. 593: 2889–2907.

Tsien JZ, Chen DF, Gerber D, Tom C, Mercer EH, Anderson DJ, Mayford M, Kandel ER, Tonegawa S. 1996. Subregion- and cell type-restricted gene knockout in mouse brain. Cell. 87: 1317–1326.

Uchigashima M, Yamazaki M, Yamasaki M, Tanimura A, Sakimura K, Kano M, Watanabe M. 2011. Molecular and morphological configuration for 2-arachidonoylglycerol-mediated retrograde signaling at mossy cell-granule cell synapses in the dentate gyrus. J Neurosci. 31:7700–7714.

Vallee M, Vitiello S, Bellocchio L, Hebert-Chatelain E, Monlezun S, Martin-Garcia E, Kasanetz F, Baillie GL, Panin F, Cathala A, et al. 2014. Pregnenolone can protect the brain from cannabis intoxication. Science. 343:94–98.

Varga EV, Georgieva T, Tumati S, Alves I, Salamon Z, Tollin G, Yamamura HI, Roeske WR. 2008. Functional selectivity in cannabinoid signaling. Curr Mol Pharmacol. 1:273–284.

Wang W, Kantorovich S, Babayan AH, Hou B, Gall CM, Lynch G. 2016a. Estrogen's effects on excitatory synaptic transmission entail integrin and TrkB transactivation and depend upon β1-integrin function. Neuropsychopharmacology. 41:2723–2732.

Wang W, Trieu BH, Palmer LC, Jia Y, Pham DT, Jung KM, Karsten CA, Merrill CB, Mackie K, Gall CM, et al. 2016. A primary cortical input to hippocampus expresses a pathway-specific and endocannabinoid-dependent form of long-term potentiation. eNeuro. 3. doi:10.1523/ENEURO.0160-16.2016.

Wen Z, Nguyen HN, Guo Z, Lalli MA, Wang X, Su Y, Kim NS, Yoon KJ, Shin J, Zhang C, et al. 2014. Synaptic dysregulation in a human iPS cell model of mental disorders. Nature. 515: 414–418.

Witter MP. 2007. Intrinsic and extrinsic wiring of CA3: indications for connectional heterogeneity. Learn Mem. 14:705–713.

Zhao J, Zheng C, Guan J. 2000. Pyk2 and FAK differentially regulate progression of the cell cycle. J Cell Sci. 113(Pt 17): 3063–3072.